

1 **Fire-precipitation interactions amplify the quasi-biennial**
2 **variability of fires over southern Mexico and Central America**

3 Yawen Liu ^{1,2}, Yun Qian ^{3*}, Philip J. Rasch ³, Kai Zhang ³, L. Ruby Leung³, Yuhang Wang ⁴,
4 Minghuai Wang ^{1,2}, Hailong Wang ³, Xin Huang^{1,2}, and Xiu-Qun Yang ¹

5 ¹School of Atmospheric Sciences, Nanjing University, China

6 ²Joint International Research Laboratory of Atmospheric and Earth System Sciences & Institute
7 for Climate and Global Change Research, Nanjing University, China

8 ³Pacific Northwest National Laboratory, Richland, Washington, USA

9 ⁴School of Earth and Atmospheric Sciences, Georgia Institute of Technology, Atlanta, Georgia,
10 USA

11 *Correspondence to:* Yun Qian ~~and Philip J Rasch and~~ (yun.qian@pnnl.gov ~~and~~
12 Philip.Rasch@pnnl.gov)

13 **Abstract.** Fires have great ecological, social, and economic impacts. However, fire prediction and
14 management remain a challenge due to a limited understanding of their role in the Earth system.
15 Fires over southern Mexico and Central America (SMCA) are a good example, which greatly
16 impact local air quality and regional climate. Here we report that the spring-peak (Apr-May) fire
17 activities in this region have a distinct quasi-biennial signal based on multiple satellite datasets
18 measuring different fire characteristics. The variability is initially driven by the quasi-biennial
19 variations of precipitation. Composite analysis indicates that strong fire years correspond to
20 suppressed ascending motions and weakened precipitation over the SMCA. The anomalous
21 precipitation over the SMCA is further found to be mostly related to the East Pacific-North Pacific
22 (EP-NP) pattern two months previous to the fire season. The positive phase of EP-NP leads to
23 enhanced precipitation over the eastern US yet suppressed precipitation over SMCA, similar to the
24 spatial pattern of precipitation difference between strong and weak fire years. Meanwhile, the
25 quasi-biennial signals in precipitation and fires appear to be amplified by their interactions through
26 a positive feedback loop on short timescales. Model simulations show that in strong fire years,
27 more aerosol particles are released and transported downstream over the Gulf of Mexico and the
28 eastern US, where suspended light-absorbing aerosols warm the atmosphere and cause ascending
29 motions of the air aloft. Subsequently, a compensating downward motion is formed over the fire
30 source region and ultimately suppresses precipitation and intensifies fires. Statistical analysis
31 shows the different duration of the two-way interaction, where the fire suppression effect by
32 precipitation lasts for more than 20 days, while fire leads to a decrease in precipitation at shorter
33 time scales (3-5 days). This study demonstrates the importance of fire-climate interactions in
34 shaping the fire activities on interannual scale and highlights how precipitation-fire interactions at
35 short timescales contribute to the interannual variability of both fire and precipitation.

36 **1 Introduction**

37 Natural and human-induced fires are key features of the Earth system (Bowman et al., 2009).
38 Uncontrolled large fires damage biodiversity, affect human health, and incur high economic costs
39 (Knorr et al., 2017; Aguilera et al., 2021; Bowman et al., 2017). Comprehensive knowledge of
40 fires' causes, variability, and climate effects is necessary to accommodate or manage fires
41 effectively, and to mitigate adverse societal impacts.

42 Changes in climate alter fire regimes (Power et al., 2008; Jolly et al., 2015), because the occurrence
43 and intensity of fires depend on meteorological factors such as precipitation, wind, and humidity
44 (Flannigan et al., 2009; Marlon et al., 2008; Abram et al., 2021; Fang et al., 2021). Fires alter
45 weather and climate as well: they are important sources of aerosol particles that modify Earth's
46 energy and water budget either by directly absorbing and scattering sunlight or affecting cloud
47 microphysical processes (Voulgarakis and Field, 2015; Jiang et al., 2020; Liu et al., 2018; Yue et
48 al., 2022; Lu et al., 2018). There are many modes of interaction. The modes are complex, operate
49 through a variety of mechanisms, and manifest on a large variety of time and space scales (Ding
50 et al., 2021; Zhang et al., 2022). For example, Huang et al. (2023) have demonstrated that synoptic-
51 scale fire-weather feedback plays a prime role in driving extreme fires in the Mediterranean and
52 monsoon climate regimes over the US West Coast and Southeastern Asia. On interannual scales,
53 fires in the maritime subcontinent have been shown to affect SSTs, land temperature as well as
54 atmospheric stability, and influence ENSO on 3-6 year timescales (Tosca et al., 2010). The
55 extreme 2019-2020 Australian fires have also been demonstrated to contribute to the 2020-2022
56 strong La Niña event by enhancing cloud albedo, cooling and drying out the air, and forming a
57 positive feedback between the northward migration of intertropical convergence zone and sea
58 surface temperature cooling in the Niño3.4 region (Fasullo et al., 2023). Moreover, on even longer
59 timescales, fires can affect the accumulation of carbon dioxide and methane by modifying global
60 features like the Hadley circulation that change precipitation and temperature patterns and
61 eventually affect forest ecosystems to produce feedback operating over decades and centuries
62 (Crutzen and Andreae, 1990; Page et al., 2002; Tosca et al., 2013). It is hence necessary to explore
63 fire characteristics with special considerations of their multi-scale variability and feedback.

64 From a global perspective, fires occur progressively more frequently towards the tropics (Mouillot
65 and Field, 2005). Tropical savanna and forest burning contribute approximately 80% of global

66 open fire emissions (Bond et al., 2013). However, tropical regions also feature a great diversity of
67 climate-weather systems that affect fire occurrence and seasonality. In the tropical Northern
68 Hemisphere, fires over tropical southern Mexico and Central America (SMCA) occur during the
69 Feb-May dry season and peak in April-May (Magi et al., 2012). These fire activities have a
70 substantial influence on local air quality and human health (e.g., over Mexico City [19-20° N, 98-
71 100°W] and the Yucatan region (Crouse et al., 2009; Yokelson et al., 2007; Yokelson et al.,
72 2009). Fire emissions over the SMCA region also affect the eastern US after long-range transport
73 (Kreidenweis et al., 2001; Lee et al., 2006; Rogers and Bowman, 2001). Understanding the
74 processes that shape fire variabilities over this region is hence important locally (for air quality
75 and fire management) and over broader regions.

76 Here, for the first time, we report a distinct quasi-biennial variability of fire activities over the
77 southern Mexico and Central America region (SMCA, 10-25°N, 80-100°W) during the peak
78 burning months (April – May) over 2003-2019 by validating different fire characteristics with the
79 use of multiple independent datasets. We further explore the dominant causes of this quasi-biennial
80 signal and provide concrete evidence for positive fire-precipitation feedback on short timescales
81 to amplify the quasi-biennial signal based on model simulations.

82 **2 Data and Methods**

83 **2.1 Observations**

84 Two sets of fire emission inventories were used to investigate the interannual variability of fire
85 activities. The Global Fire Emissions Database with small fires version 4.1 (GFED v4.1s) is a
86 bottom-up inventory that generates fire-consumed dry matter using fire-burned areas combined
87 with emission factors (Giglio et al., 2013; Randerson et al., 2012). GFED v4.1s provides monthly
88 mean fire-consumed dry matter in total and for individual fire types at 0.25-degree spatial
89 resolution. The Quick Fire Emissions Dataset (QFED) is a top-down emission inventory that
90 generates fire emissions by using empirical relationships between fire-consumed dry matter and
91 fire radiative power (Koster et al., 2015). Daily emissions of fire-emitted species at 0.1 horizontal
92 resolution from QFED version 2.5 were examined. Since the interannual variations of different
93 species are consistent, only variation of fire-emitted black carbon (BC) is shown here. We focused
94 on the fire activities after 2003 to exclude the influence of the extremely strong ENSO events,

95 specifically the 1997/1998 El Niño event and the subsequent 1998-2000 La Niña event, which are
96 among the most powerful ENSO events in recorded history.

97 We also examined the interannual variation of fire-induced changes in aerosol optical depth based
98 on the MERRA-2 reanalysis data (Gelaro et al., 2017) and Level 3 version 4.2 CALIPSO satellite
99 dataset (Winker et al., 2013). For the MERRA-2 data, monthly mean BC aerosol optical depth
100 (AOD) was used for a better comparison with the BC emission from QFED emission data. The
101 CALIPSO product divides aerosol into six sub-types, and the gridded monthly mean 532nm AOD
102 for the biomass burning aerosol type under all-sky conditions was analyzed. We used the MODIS
103 version 6.1 gross primary productivity (GPP) product (MOD17A2H, (Running, 2021)), which
104 measures the growth of the terrestrial vegetation as a proxy for fuel load. A cumulative 8-day
105 composite of GPP values is provided with a 500m pixel size. The average of GPP in the month
106 (March) prior to the burning season is examined. Interannual variations in the shortwave diffuse
107 radiative fluxes at surface, which is closely related to photosynthesis rates and primary
108 productivity is also analyzed using the photosynthetically active radiation from the Earth's Radiant
109 Energy System (CERES) product (Su et al., 2007).

110 In order to investigate the climate influence on fire activities, we analyzed monthly mean
111 temperature and maximum temperature from the Climatic Research Unit gridded Time Series
112 (CRU TS) version 4.06 (Harris et al., 2014). The dataset is constructed based on station
113 observations and provides monthly data over the global land surface at 0.5-degree resolution. Apart
114 from the CRU dataset, two sets of satellite observations of precipitation were analyzed: the
115 monthly Integrated Multi-satellitE Retrievals for GPM (IMERG) precipitation estimates at 0.1
116 degrees (Huffman et al., 2015) and the 1-degree daily (version 1.3), 2.5-degree monthly
117 (version2.3) Global Precipitation Climatology Project (GPCP) precipitation estimates (Adler et al.,
118 2018; Adler, 2017). IMERG is intended to intercalibrate and merge satellite microwave
119 precipitation estimates together with microwave-calibrated infrared satellite estimates and
120 precipitation gauge analyses (Huffman et al., 2020). Monthly mean 500hPa vertical velocity (ω)
121 at 2.5 degrees from NCEP/NCAR reanalysis (Kanamitsu et al., 2002) and 10m wind speed at 0.25
122 degrees from ERA5 reanalysis (Hersbach et al., 2020) were ~~also~~ used in our work. We also
123 calculated near surface relative humidity and vapor pressure deficit following Chiodi et al. (2021)
124 with the use of 2m temperature and dew point temperature from ERA5 reanalysis data. In order to

125 understand the interannual variation of precipitation, we examined the relationship between
126 precipitation and ten different teleconnection patterns, including Atlantic Meridional Mode
127 (AMM), East Pacific/North Pacific Oscillation (EP/NP), ENSO, North Atlantic Oscillation
128 (NAO), North Tropical Atlantic index (NTA), Pacific North American index (PNA), Tropical
129 Northern Atlantic index (TNA), Tropical Southern Atlantic index (TSA), Western Hemisphere
130 warming pool (WHWP), Quasi-biennial Oscillation (QBO). These indices and their detailed
131 definitions can be obtained from <https://psl.noaa.gov/data/climateindices/list/>.

132 **2.2 Model experiment**

133 The CESM2.1.0 model with the Community Atmosphere Model version 6 (CAM6) (Danabasoglu
134 et al., 2020) was used to investigate the feedback of fire-emitted aerosols on precipitation. The
135 F2000 component set was used with the prescribed sea surface temperature in the year 2000. The
136 horizontal resolution is set as 0.9-degree latitude by 1.25-degree longitude with 32 vertical levels.
137 Two groups of simulations were conducted. Each was driven by the representative fire emissions
138 in strong and weak fire years and referred to as Case_Strong and Case_Weak. The difference in
139 variables (e.g., temperature and precipitation) between the two cases (Case_Strong minus
140 Case_Weak) indicate the influence, or difference in feedback, caused by stronger fire emissions.
141 As our work focused on the influence of fire activities over SMCA, only fire emissions over the
142 SMCA region were considered. Since fire emissions and anthropogenic emissions are specified
143 separately in the CESM2 model, we modified the default fire emission inventory (Van Marle et
144 al., 2017) in CESM2.1.0 accordingly while global anthropogenic emissions were kept unchanged
145 and remained the same between cases. Given that composite analysis indicates fire emissions in
146 weak fire years are approximately half those in strong fire years. We simply used the average of
147 fire emissions during strong fire years in Case_Strong, and reduced these by half in Case_Weak.
148 More subtle changes in fire locations between strong and weak fire years are hence ignored.
149 Furthermore, global climate models have long been found to underestimate fire-induced changes
150 in aerosols (Zhong et al., 2022). Hence, in order to ensure the simulated difference in fire-induced
151 AOD between Case_Strong and Case_Weak is comparable to observations, the default inventory
152 is multiplied by a factor of 3 to ensure the simulated fire-induced AOD changes are comparable to
153 observations. For each group, 9 ensemble simulations were performed with slight differences in
154 their initial conditions. The ensemble mean is calculated as the average of 9 members. All

155 simulations start on Jan.1 with a 3-month spin-up time. The T-test is used to identify statistically
156 significant differences between Case_Strong and Case_Weak.

157 **3 Results**

158 **3.1 Biennial variability of fire activities**

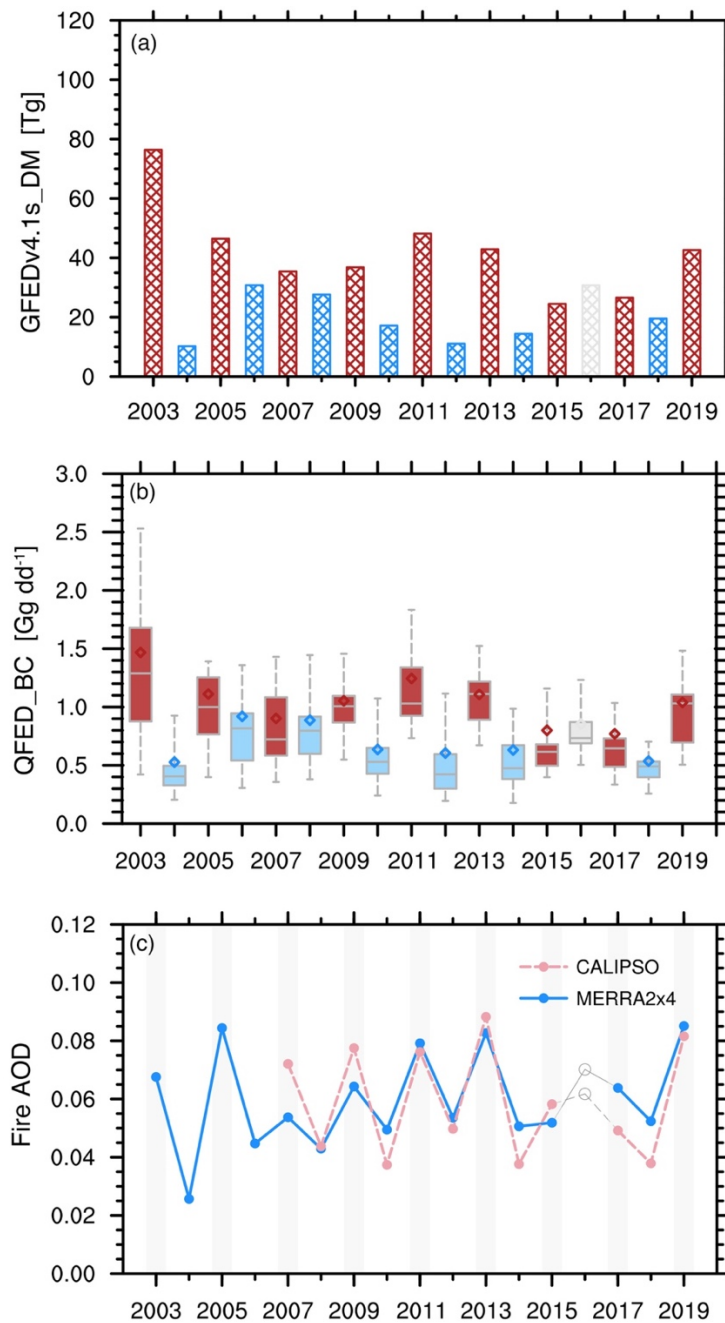
159 We focus on the southern Mexico and Central America region (SMCA) covering both the Yucatan
160 region and Mexico City. Major fire types in this region consist of deforestation fires, savanna fires,
161 and agricultural waste burning, which respectively are estimated to consume 45.5%, 42.1%, and
162 12.40% of the total burned dry matter during the peak burning months (Apr-May) of the 17-year
163 (2003-2019) study period.

164 As shown in Fig. 1a, GFEDv4.1s estimates of the regional sum of the total dry matter consumed
165 by fire activities feature obvious quasi-biennial variability. Generally speaking, fire activities in
166 odd-numbered years show higher consumption of dry matter than adjacent even-numbered years
167 with the only exception of the year 2016, which might be related to a long-lasting El Niño event
168 spanning 2014-2016. Composites of fire consumption of dry matter indicate enhanced fire
169 activities along both sides of the high terrains in odd-numbered years, and the most profound
170 difference appears over the bordering area between southern Mexico and Guatemala (Fig. S2). The
171 average fire-consumed dry matter here differs by more than a factor of 6 between odd-numbered
172 and even-numbered years.

173 The quasi-biennial variability of fire activities is also evident when examining fire emissions of
174 typical fire-emitted species based on the QFED inventory (Fig. 1b). Similarly, fire-emitted BC in
175 odd-numbered years is higher than those in the adjacent even-numbered years, when considering
176 both regional mean and medium values. Furthermore, among the 9 odd-numbered years, fire
177 activities in years 2003/2011/2013 show the highest three BC emission, which is also consistent
178 with results from the GFEDv4.1s dataset. Hence, the two independent fire emission inventories
179 agree on the interannual variation of fire activities.

180 Apart from cross-checking different fire emission inventories, we further validated the variability
181 of fire activities by investigating fire-induced changes in AOD (Fig. 1c). BC AOD from MERRA-
182 2 reanalysis and AOD of biomass burning aerosol type from CALIPSO were adopted to represent
183 fire activities. Basically, the interannual variation of fire-related AOD in both datasets agrees well
184 with the estimates from fire inventories, thus providing additional support for the quasi-biennial

185 variability of fire activities in the peak burning months over SMCA. Overall, the intercomparison
186 between multiple datasets indicates a consistent quasi-biennial variability in different fire
187 characteristics, including fire-consumed dry matter, fire-emitted aerosols as well as fire-related
188 changes in optical properties. Note that among the four datasets, the GFEDv4.1s inventory and
189 MERRA-2 reanalysis data provide data till the year of 2023, and the quasi-biennial variability in
190 the extended time series remains robust till 2023 (Fig. S1). To describe this quasi-biennial
191 variability for convenience, we hereafter refer to the odd-numbered (even-numbered) years that
192 have higher (lower) fire consumptions of dry matter than adjacent years as strong (weak) fire years.
193



195
 196
 197
 198
 199
 200
 201
 202
 203
 204
 205
 206

Figure 1. Interannual variations of different fire characteristics during the peak burning season (Apr-May) over Southern Mexico and Central America (SMCA). (a) Regional sum of the total dry matter consumed by fire activities based on the GFEDv4.1s emission data. (b) Distributions of the daily sum of fire-emitted black carbon (BC) over SMCA based on QFED emission data. Boxes denote the 25th and 75th percentiles. Bars outside the boxes denote the 10th and 90th percentiles. Bars within the boxes denote the medium values, and dots denote regional mean values (c) Regional mean aerosol optical depth (AOD) of smoke aerosols from CALIPSO product and BC AOD from MERRA-2 reanalysis. The odd-numbered years with strong fires are denoted by the grey bars.

207 **3.2 Dominant role of the biennial variability of precipitation**

208 Fire activity is strongly affected by factors including fire ignition, fuel load, and climate-weather
209 conditions (Flannigan et al., 2005; Archibald, 2016; Ichoku et al., 2016; Veira et al., 2016). Fire
210 ignition is affected by both natural lightning and human activities (Pechony and Shindell, 2009).
211 Since there is no policy to regulate fire activities with periodicity, it is unlikely that human impact
212 is the major driving force. Fuel availability may play a role in the interannual variation of fires.
213 After having examined the GPP (surrogate for fuel load) prior to the burning season, we found
214 little evidence regarding the role of fuel availability in contributing to the interannual variation of
215 fires (Fig. S3). Lower values of GPP are found in some strong fire years compared to their adjacent
216 years, e.g., the years 2003 and 2005. Correlations between regional GPP and fire-consumed dry
217 matter are even slightly negative. Moreover, correlations between the regional mean diffuse
218 radiative flux and fire-consumed dry matter are also statistically insignificant.

219 Close yet complex relationships between ambient conditions (e.g., humidity, temperature,
220 precipitation) and fire activities have been widely revealed in previous studies (Cary et al., 2006;
221 Gillett et al., 2004; Prasad et al., 2008). For example, warm temperatures could increase fire
222 activity by increasing evapotranspiration and also by lengthening fire duration, while both the
223 timing and amount of precipitation could regulate fire behavior. To identify the climatic factors
224 that might be responsible for the quasi-biennial variation of fire activities, we first examined the
225 relationships between fire-consumed dry matter and different meteorological variables (Table 1).
226 Temporal correlations of their regional mean values indicate that fire activities are enhanced with
227 warmer mean and maximum temperature ($R=0.47$ and 0.59), but are weakened with higher
228 precipitation ($R=-0.69$). Though wind speed could affect the spread of fire activities, the
229 insignificant correlation signifies a minor influence on the interannual scale (Fig. S3). Other
230 meteorological metrics such as vapor pressure deficit (VPD) and relative humidity (RH) are also
231 frequently used to help understand fire-meteorology interactions. Here Correlations in Tabel 1
232 indicate that we found higher VPD facilitates fire activities while higher RH depresses fire
233 activities. Here we found that the interannual variations of regional mean VPD and RH are in fact
234 highly correlated with precipitation ($R = -0.8$ for VPD and $R=0.7$ for RH, respectively) and
235 temperature ($R = 0.7$ for VPD and $R = -0.5$ for RH, respectively) over the SMCA region.

236 Figure 2 shows the spatial distribution of correlations of fire-consumed dry matter with
237 precipitation and mean temperature during peak burning months. With respect to precipitation,

238 negative correlations cover almost the entire SMCA region and are statistically significant over
 239 major fire source areas from Yucatan extending southwestward to Chiapas. In contrast, positive
 240 correlations between fire-consumed dry matter and maximum temperature mainly appear over the
 241 northern part of SMCA (southern Mexico), albeit with less influence over Central America (e.g.,
 242 fire source areas in Guatemala). Hence, the interannual variability of precipitation affects the
 243 variation of fire activities on a wider spatial range. We next examined closely the time series of
 244 regional mean precipitation and temperature (Fig 3). Here regional mean values are calculated
 245 using data over land so that only climate conditions that could directly affect fire activities are
 246 considered. Two independent precipitation datasets show similar temporal evolution patterns. An
 247 obvious quasi-biennial variability is seen in regional mean precipitation. More suppressed
 248 precipitation (compared to adjacent years) corresponds well to the strong fire years (excluding the
 249 year 2016). Furthermore, spectral analysis confirms a statistically significant periodicity of
 250 approximately 2 years (0.042 cycles per month) for precipitation, suggesting the mediation of
 251 precipitation on the quasi-biennial feature of fire activities. Meanwhile, the quasi-biennial signal
 252 is less apparent in mean and maximum temperatures. For instance, temperatures in the strong fire
 253 years 2007 and 2009 are smaller in magnitude compared to adjacent weak fire years. Nevertheless,
 254 higher mean and maximum temperatures (compared to adjacent years) appear in 2003 and 2011,
 255 which combines with the suppressed precipitation, contributing to the abnormally high fire-
 256 consumed dry matter in the two years. As a result, while both temperature and precipitation are
 257 critical in shaping fire activities over the SMCA region, precipitation plays a more fundamental
 258 role in formulating the quasi-biennial variability of fires.

259

260 **Table 1.** Correlations between the regional sum of fire consumed dry matter based on the
 261 GFEDv4.1 data and regional mean values of different meteorological variables (including the
 262 monthly mean precipitation from IMERG dataset, mean temperature, maximum temperature from
 263 CRU dataset, and 10m wind speed from ERA5 reanalysis) averaged in the peak fire season (April-
 264 May).

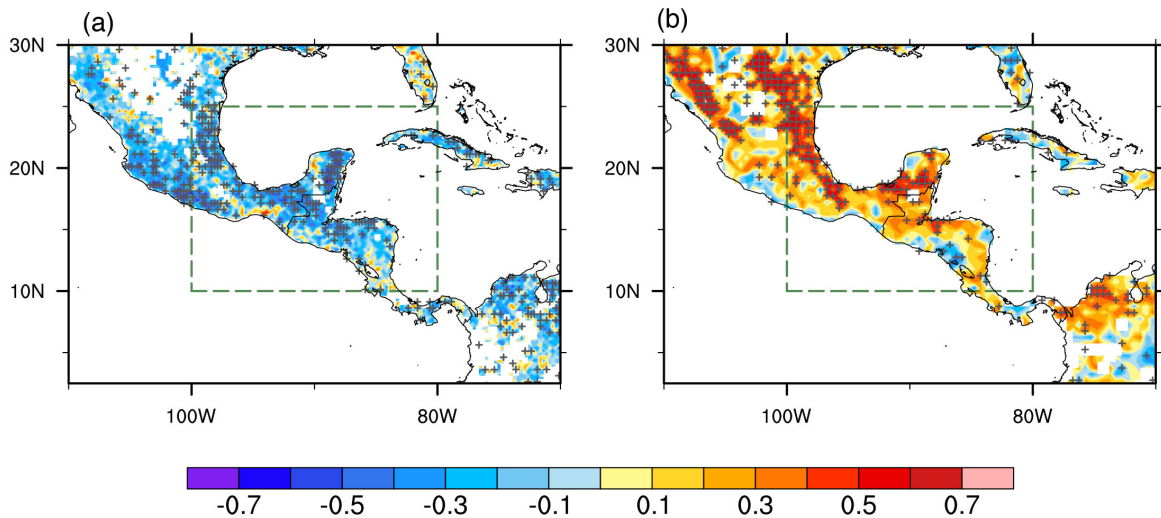
Correlation	Precipitation	Mean Temperature	Maximum Temperature	<u>Relative humidity</u>	<u>Vapor pressure deficit</u>	10m wind speed
Fire-consumed Dry matter	-0.69*	0.47*	0.59*	<u>-0.63*</u>	<u>0.61*</u>	0.29

265 * represents the correlations are statistically significant at the 90% confidence level based on the
266 student's T-test.

267

268

269



270

271

272

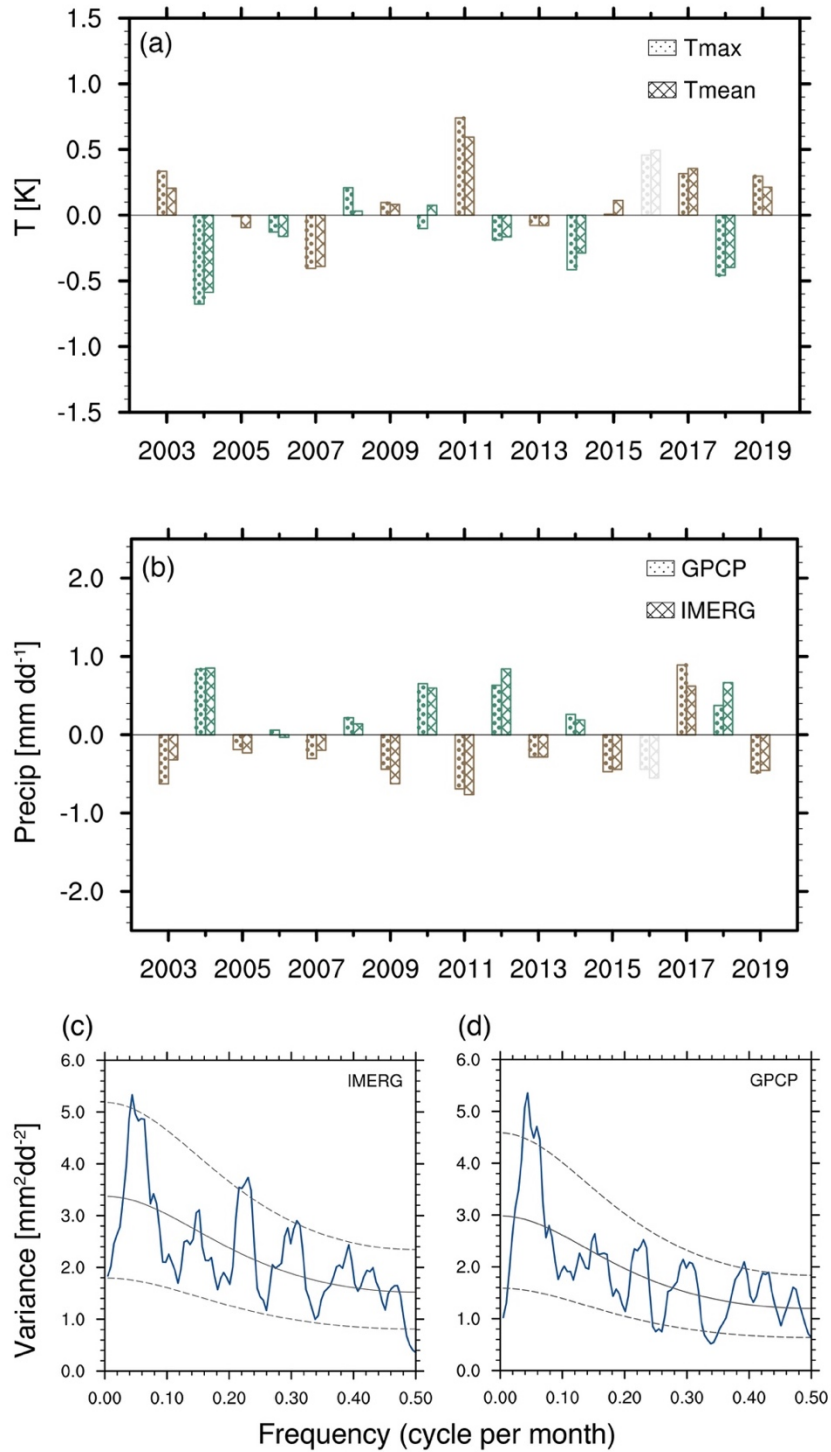
273

274

275

276

Figure 2. The influence of meteorological factors on fire activities over SMCA. Spatial distributions of grid-to-grid correlations between fire-consumed dry matter and (a) precipitation from IMERG and (b) maximum temperature from CRU during the peak fire season (Apr-May) over 2003-2019. Stippling indicates the correlations are statistically significant at the 90% confidence level based on the student's T-test. The green boxes denote the SMCA region.



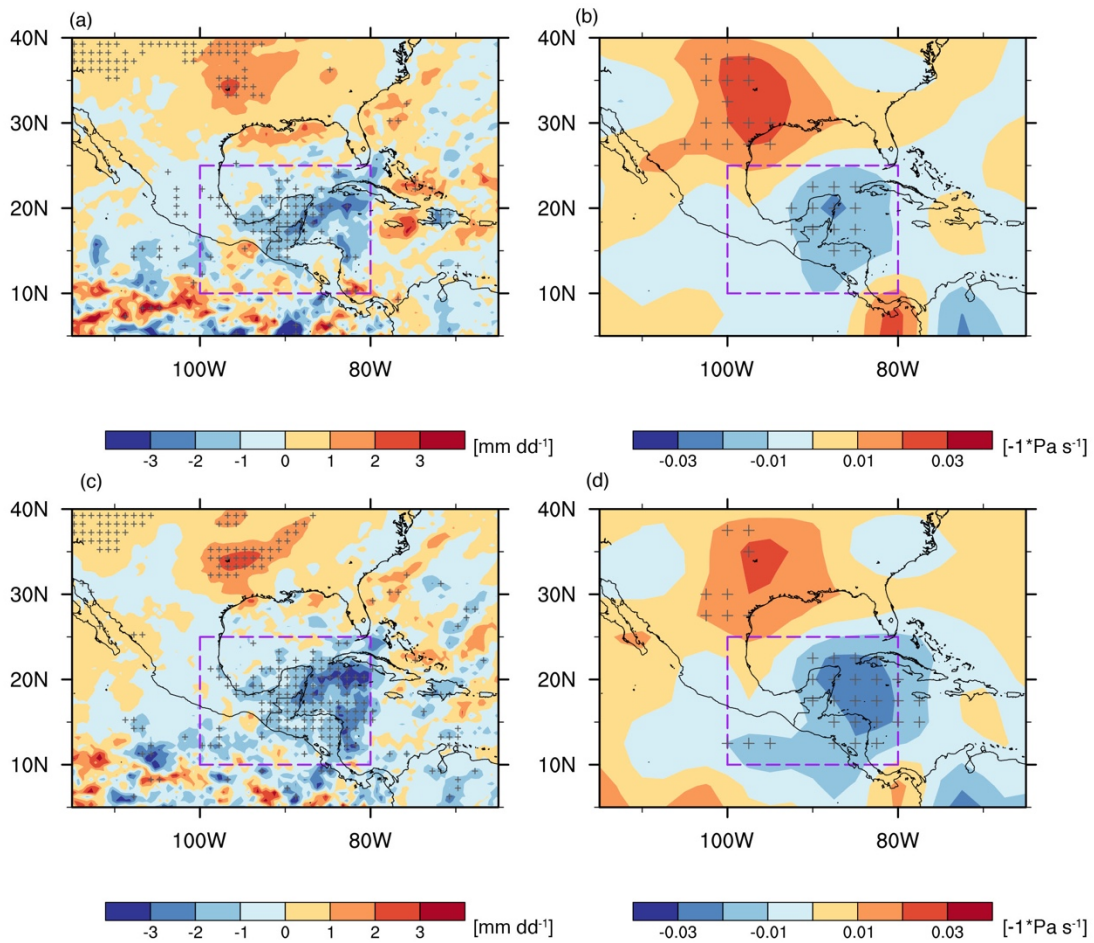
277
 278
 279
 280
 281
 282
 283
 284

Figure 3. Interannual variability of meteorological factors in peak fire season over SMCA. Time series of the Apr-May (a) mean/maximum temperature and (b) mean precipitation anomalies (with respect to the 2003-2019 climatology mean) averaged over SMCA (land only). (c) Spectral analysis of monthly mean precipitation averaged over SMCA during 2003-2019. The black solid line and dashed lines represent the red noise curve and the 10%, 90% confidence interval.

285 The leading role of precipitation on the interannually varying fire activities is evident in the
286 composite analysis, as shown by the contrast of reduced precipitation in strong fire years and
287 enhanced precipitation in weak fire years (Fig. 4a). The composite analysis further shows that the
288 anomalous precipitation is closely related to vertical motions, with stronger subsidence
289 corresponding to weaker precipitation (Fig. 4b). It is worth noting that to the northwest of the
290 SMCA region near the southeast US, composited precipitation and vertical velocity also differ
291 significantly between strong and weak fire years albeit of opposite signs. Consistent changing
292 features of precipitation and vertical velocity are also captured when regressing the two variables
293 on the regional mean precipitation over SMCA (Fig. 4c-d). The negative regression coefficients
294 indicate a stronger upward (downward) motion corresponding to higher (weaker) precipitation. In
295 sum, for a specific year, stronger subsidence and the subsequent suppression of precipitation tend
296 to amplify fire activity in that year, and vice versa for the year with weakened subsidence and less
297 suppression effect of precipitation. In this way, the quasi-biennial variability of precipitation leads
298 to the same interannual variability of fire activities.

299 Precipitation patterns over the SMCA region and the variability are associated with complex
300 physical forcing mechanisms, e.g. changes in sea surface temperature, low-level winds, the
301 strength and position of ITCZ et al., and all of these processes could be modulated by large-scale
302 modes of atmospheric and oceanic variability (Duran-Quesada et al., 2017; Perdigon-Morales et
303 al., 2019; Amador et al., 2006). Here we chose 10 typical teleconnection patterns, for example, the
304 El Niño-Southern Oscillation, (ENSO), based on previous studies and examined their relationships
305 with SMCA precipitation in the peak fire months. After calculating the correlations between Apr-
306 May mean precipitation and the index in varying months (both simultaneously and previous to the
307 fire season), we found that the precipitation in the fire season is mostly affected by the East
308 Pacific/North Pacific Oscillation (EP/NP) pattern in the previous two months (Feb-Mar).
309 Generally, the positive phase of EP/NP features negative height anomalies and an enhanced
310 cyclonic circulation over the eastern United States (Athanasiadis et al., 2010). Consequently, in
311 the following fire season, this causes anomalous upward and downward motions over the
312 southeastern US and the SMCA region respectively (Fig. S4), and enhances precipitation over the
313 southeastern US yet suppressing precipitation over the SMCA region (Fig. 5). Hence, the EP/NP
314 teleconnection results in an opposite responding pattern in precipitation and vertical velocity

315 between the eastern US and the SMCA region. This further explains the similar contrasting spatial
 316 pattern that is found in the aforementioned composite and regression analysis.

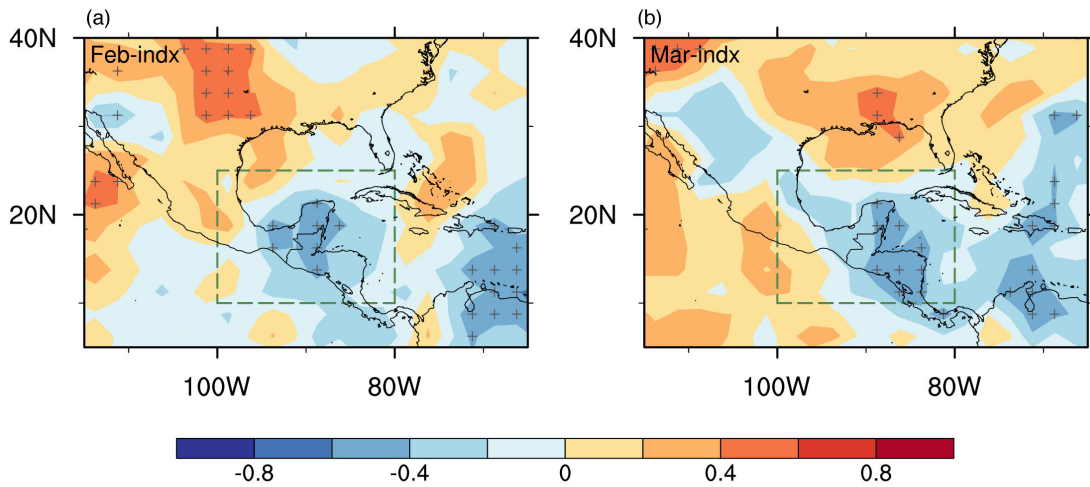


317
 318

319 **Figure 4.** Varying characteristics of precipitation and circulations. Differences of composites of
 320 (a) precipitation and (b) 500hPa vertical pressure velocity (reversed signs) between strong and
 321 weak fire years. Stippling indicates the differences are statistically significant at the 90%
 322 confidence level based on T-test. Regressions of Apr-May mean (c) precipitation and (d) 500hPa
 323 vertical velocity on the regional mean precipitation over SMCA (reversed signs) during 2003-
 324 2019. Stippling indicates regression coefficients are statistically significant at the 90% confidence
 325 level based on the T-test.

326

327



328

329

330

331

332

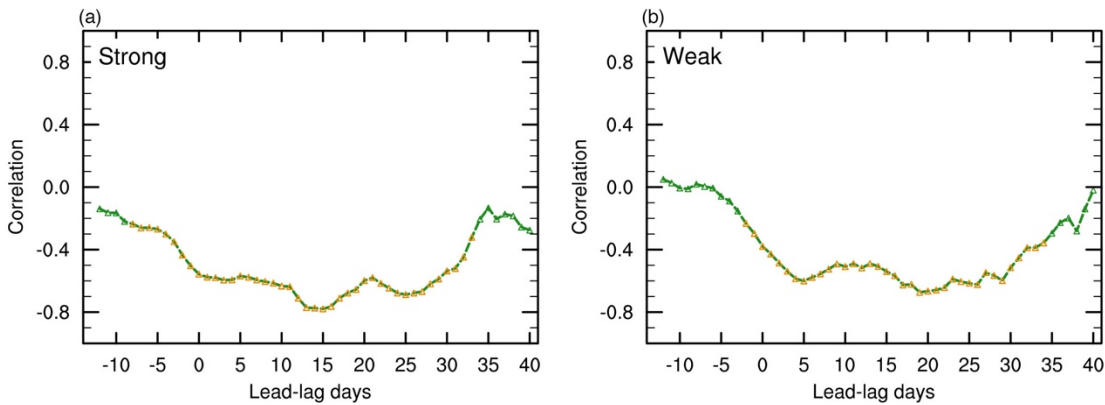
333

334

335

Figure 5. Influence of the EP/NP teleconnection pattern on precipitation in peak fire season. Spatial distributions of correlations of EP/NP index in (a) February and (b) March with the mean precipitation in the peak fire season (Apr-May) during 2003-2019. Stippling indicates the correlations are statistically significant based on the student's T-test.

336



337

338

339

340

341

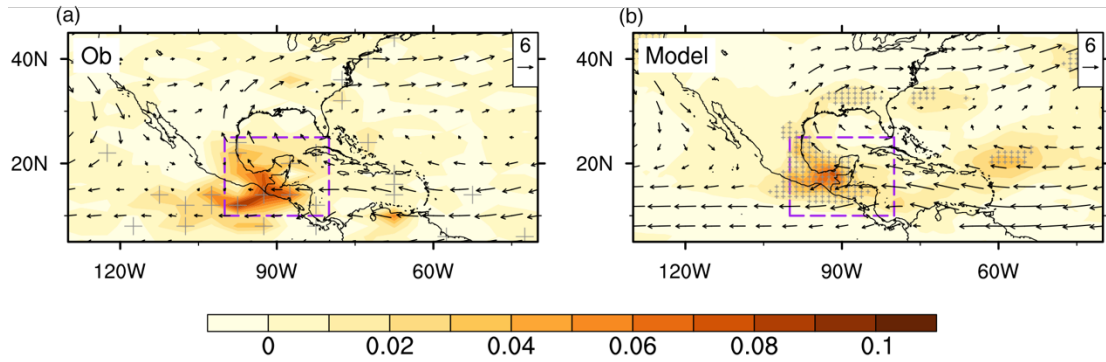
342

Figure 6. Different duration of fire-precipitation interaction. Lead-lag correlations between regional mean daily precipitation and fire emission composites in (a) strong fire years and (b) weak fire years over SMCA. Positive lead-lag days represent that precipitation leads while negative lead-lag days represent fire emissions leads. Correlations that are statistically significant at the 90% confidence level based on Student's t-test are marked with yellow triangles.

343 **3.3 Positive feedback between enhanced fire emissions and suppressed precipitation**

344 Previous studies have found that fire-emitted aerosols could interact with synoptic weather, which
345 in turn affects fire variability (Huang et al., 2023). In view of this, one concern is if fire and
346 precipitation interact on short timescales (i.e., within individual fire seasons) in our case over the
347 SMCA region, and if so, how this feedback modulates the quasi-biennial variability of
348 precipitation and fire activities. We first calculated lead-lag correlations between daily
349 precipitation and fire emissions to identify the short-term fire-precipitation interaction. As shown
350 in Fig. 6 lead-lag correlations between regional mean precipitation and fire emission are generally
351 similar whether fire activities in strong or weak fire years are considered. When precipitation leads,
352 precipitation negatively correlates with fire emission for more than 20 days, signifying a long-
353 lasting suppression effect of precipitation on fire activities. In other words, weakened precipitation
354 would enhance fire activities. Meanwhile, when fire leads, negative correlations indicate that
355 increased fire activities would further suppress precipitation at shorter timescales (3-5 days)
356 through rapid adjustments. In short, there is a two-way interaction between precipitation and fire
357 activities on short timescales with different duration, forming a positive feedback loop.

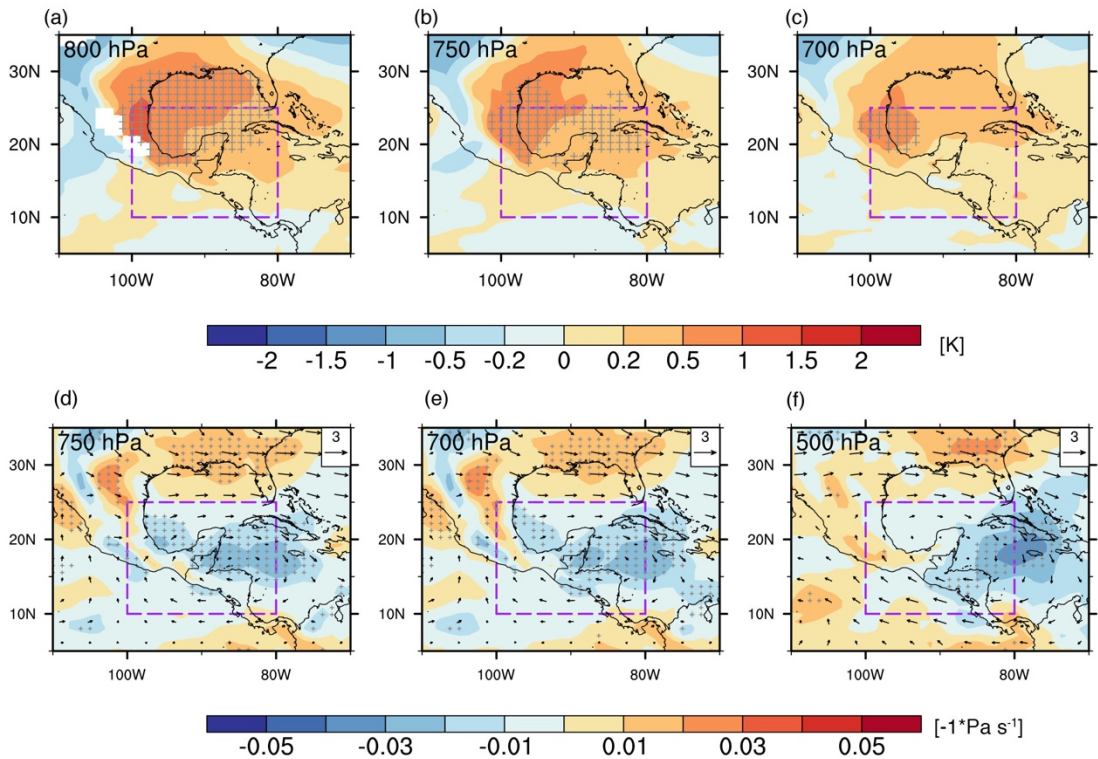
358 We also conducted sensitivity simulations to investigate the underlying processes involved in the
359 fire-precipitation feedback. Fig. 7 shows the simulated difference in AOD (referred to as fire AOD)
360 between Case_Strong and Case_Weak. Both the spatial pattern and magnitude agree well with the
361 difference in AOD between strong and weak fire years based on CALIPSO observations.
362 Compared to the spatial patterns of fire consumption in Fig. 7, we can clearly see two transport
363 pathways of fire-emitted aerosols due to the continental divide by the Central Mexican Plateau.
364 North of 15°N, fire-emitted aerosols are transported northward by the subtropical high, among
365 which large amounts accumulate over the downstream Gulf of Mexico due to the block of the high
366 terrain, and the rest is further transported northward reaching the southeastern US; South of 15°N,
367 prevailing easterlies transport fire-emitted aerosols directly westward, far away to the eastern
368 Pacific.



369
370

371 **Figure 7.** Evaluation of model simulated fire-induced AOD. (a) Spatial distributions of differences
372 in biomass burning AOD between strong and weak fire years from CALIPSO satellite data. (b)
373 Differences in simulated AOD between Case_Strong and Case_Weak. Mean 850hPa wind vectors
374 from (a) NCEP reanalysis data averaged in all years and (b) model simulations averaged between
375 both cases are overlaid respectively. Stippling indicates the differences in AOD are statistically
376 significant based on T-test.

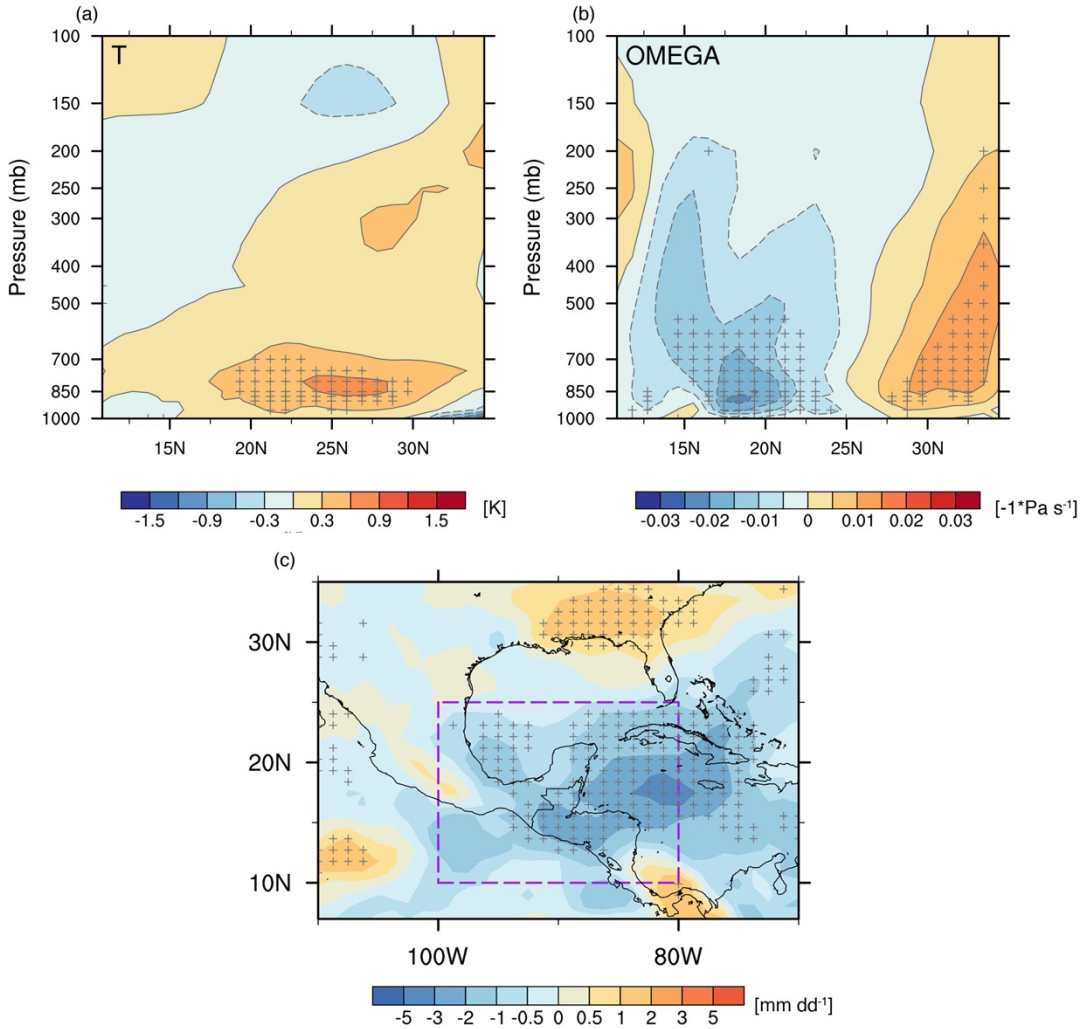
377



378
379

380 **Figure 8.** Changes in meteorological variables induced by fire-emitted aerosols. Differences in (a-
381 c) atmospheric temperature and (d-f) vertical pressure velocity (reversed signs and shaded colors)
382 at different vertical levels between Case_Strong and Case_Weak. Changes in horizontal winds
383 between the two cases are overlaid in (d-f). Stippling indicates the differences are statistically
384 significant at the 90% confidence level based on T-test.

385 Considering the northward pathway, with the stack of light-absorbing BC aerosols, air temperature
386 warms up by approximately 1-2K, and this warming extends from 800hPa to 700hPa where BC
387 aerosols suspend (Fig. 8a-c). Vertical slices of the temperature anomalies indicate significant
388 warming to the north (downstream) of the fire source regions (Fig. 9a). In response to this warming,
389 the air above the fire aerosol layers rises up (Fig. 8d-f). The anomalous ascending motion covers
390 from the Gulf of Mexico to the southeastern US, with the maximum center located near the Gulf
391 of Mexico. This abnormal ascending motion, on one hand, enhances precipitation downstream of
392 the fire source regions, and on the other hand forces a compensating anomalous descending motion
393 over the SMCA region and suppresses the precipitation over the fire source regions (Fig. 9b-c).
394 This simulated opposite change in precipitation resembles the spatial pattern of the composited
395 precipitation difference between strong and weak fire years (Fig. 4a), suggesting that fire-
396 precipitation interaction reinforces the contrast of precipitation between strong and weak fire years.
397 Therefore, the model simulations confirm a positive fire-precipitation feedback loop on the short
398 timescale within the fire season. Though variations of RH could influence fire activities on
399 interannual scales, the short-term feedback of fire aerosols on near surface RH are much weaker
400 compared to precipitation (Fig. S5).



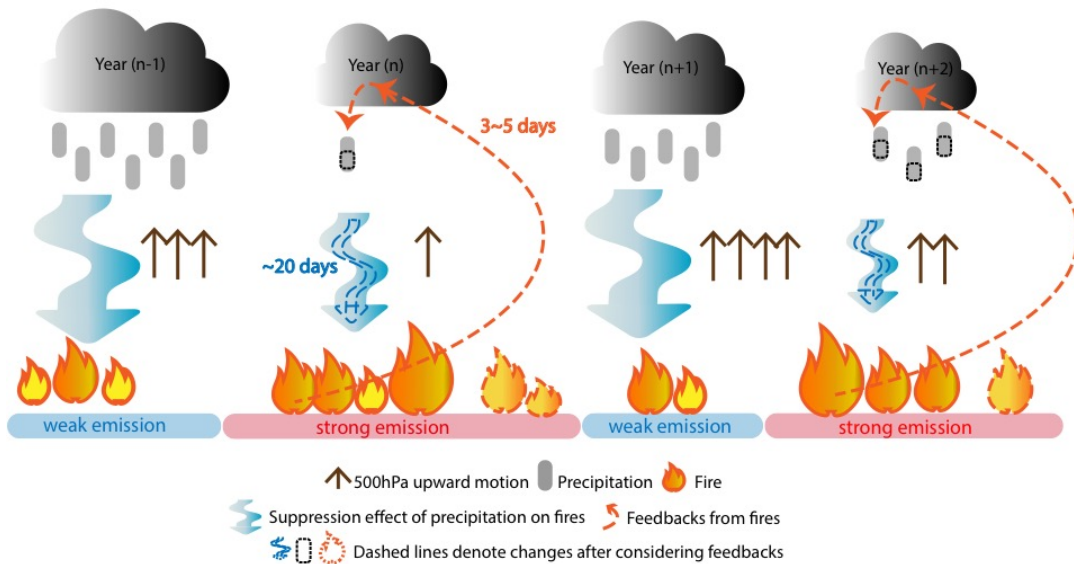
401
 402
 403 **Figure 9.** Vertical slices of differences in (a) atmospheric temperature and (b) pressure velocity
 404 averaged along $[80^\circ - 100^\circ \text{W}]$ between Case_Strong and Case_Weak. (c) Differences in
 405 precipitation between Case_Strong and Case_Weak. Stippling indicates the differences are
 406 statistically significant based on T-test.

407
 408 As illustrated in Fig. 10, originally on the interannual scale, fire activities over the SMCA region
 409 exhibit a significant quasi-biennial variability that is predominantly determined by the quasi-
 410 biennial variation of precipitation. On this basis, there is an additional two-way interaction between
 411 fire and precipitation on short timescales. Typically, precipitation suppresses fire activities with a
 412 time lag of more than 20 days, while fire-emitted aerosols suppress precipitation by modifying
 413 circulations with a timescale of 3-5 days. That is to say, for a year with abnormally weak
 414 precipitation, fire activities would get amplified, which in turn further weakens precipitation. In

415 this way, the short-term positive feedback loop ultimately enhances the quasi-biennial variability
 416 of precipitation and fire activities over the SMCA region.

417

418



419

420 **Figure 10.** A schematic diagram illustrating how multi-scale fire-precipitation interactions shape
 421 the quasi-biennial variability of fires over SMCA. On the interannual scale, the quasi-biennially
 422 varying precipitation triggers a similar quasi-biennial variability of fire activities via its
 423 suppression effect. Compared to adjacent years, a weaker precipitation year will facilitate stronger
 424 fires. On short timescales within each fire season, there is a positive feedback loop between fire
 425 and precipitation (denoted by dashed lines). The suppression effect of precipitation lasts long for
 426 approximately 20 days, while fires affect precipitation through a rapid adjustment of 3-5 days. In
 427 the weaker precipitation year, stronger fire activities emit more aerosols, which by mediating
 428 temperature and circulations, ultimately suppress precipitation over the fire source region. Such
 429 short-term interactions between precipitation and fire amplify the magnitude of anomalous fire and
 430 precipitation in individual years and enhance the quasi-biennial variability of both precipitation
 431 and fire.

432 **4 Conclusion and Discussion**

433 Fires play an important role in the Earth system, and the complex interaction between fire activities
434 and ambient conditions poses a great challenge to fire prediction and management. This study
435 identifies a distinct quasi-biennial variability of fire activities over the SMCA region during 2003-
436 2019 on the basis of different fire metrics. Both the bottom-up (GFEDv4.1s) and top-down(QFED)
437 emission inventories show relatively higher fire consumption (or emission) in the odd-numbered
438 years than the adjacent even-numbered years with the only exception of the year 2016. Moreover,
439 fire-induced changes in AOD also reveal consistent quasi-biennial variation.

440 By examining the relationships between fire consumption and different meteorological variables,
441 our analysis indicates that the quasi-biennial signal is dominated by the quasi-biennially varying
442 precipitation, while the influence of temperature is mostly reflected in a few extremely strong fire
443 years. Typically, strong fire years correspond to suppressed upward motions and weakened
444 precipitation. The quasi-biennial variability of precipitation is seen in the time series of the regional
445 mean precipitation over SMCA and the spectral analysis, and is closely related to the EP-NP
446 teleconnection pattern in the two months previous to the fire season. The positive phase of the EP-
447 NP pattern implies enhanced precipitation over the southeastern US (downstream of the SMCA),
448 albeit reduced precipitation over the SMCA region.

449 On the other hand, we further found that positive feedback exists between fire-emitted aerosols
450 and precipitation on short timescales and acts to amplify the quasi-biennial oscillations in both fire
451 and precipitation over the SMCA region. Lead-lag correlations between daily fire emission and
452 precipitation suggest that the two-way interactions occur with different duration. The suppression
453 effect of precipitation lasts for approximately 20 days, while fire-emitted aerosols weaken
454 precipitation through rapid adjustments of 3-5 days. Furthermore, model simulations reveal that
455 compared to weak fire years, more fire-emitted aerosols are transported downstream and
456 accumulate near the Gulf of Mexico in strong fire years. These suspended light-absorbing BC
457 aerosols warm the low-level atmosphere by 1-2K and induce anomalous ascending motion aloft
458 700hPa. A compensating descending motion is subsequently forced over the SMCA region, which
459 ultimately suppresses the precipitation over the fire source region and hence forms a positive
460 feedback loop.

461 These findings provide useful information relevant to the fire control and mitigation of air quality
462 over the SMCA region. Given that fire activities over the SMCA represent a typical tropical fire
463 regime, our work may also provide new insight into some fundamental features of fires in the Earth
464 System. The mechanism may also operate elsewhere useful on the planet. While precipitation is
465 demonstrated to play the primary role in determining the periodicity of fire activities over the
466 SMCA region, the fundamental cause of the quasi-biennial variability of precipitation is unknown.
467 Currently, we have only shown that the EP-NP teleconnection, among all selected indexes, exerts
468 the most influence on the interannual variability of precipitation. Other teleconnection patterns,
469 e.g., ENSO, despite their insignificant correlations with SMCA precipitation, may affect the
470 circulation and precipitation over the southeastern US or over the neighboring Intra-American Sea
471 (Anthony Chen and Taylor, 2002), and hence might more or less affect the precipitation over the
472 SMCA region. Moreover, though we demonstrated positive feedback between fire-emitted
473 aerosols and precipitation exists on short timescales, to what extent this feedback contributes to
474 the quasi-biennial variability of fire activities remains unquantified due to the absence of coupled
475 fire-climate interactions in current model simulations. Future efforts to quantify how different
476 factors and feedback work together to shape the quasi-biennial variability of precipitation and fire
477 activities using interactive fire-climate models would further benefit the prediction and
478 management of fire activities over the SMCA region.

479 **Data availability**

480 The GFED v4.1s fire emission data is available at <http://www.globalfiredata.org/data.html>.
481 The CRU TS v.4.06 can be found at <https://crudata.uea.ac.uk/cru/data/hrg/>. The QFEDv2.5 data
482 can be found at <http://ftp.as.harvard.edu/gcgrid/data/ExtData/HEMCO/QFED/v2018-07/>. The
483 MODIS GPP data is available from
484 <https://lpdaac.usgs.gov/products/mod17a2hv061/>The MERRA-2 reanalysis data can be found at
485 https://gmao.gsfc.nasa.gov/reanalysis/MERRA-2/data_access/. The IMERG precipitation dataset
486 can be obtained from <https://gpm.nasa.gov/data/imerg>. The GPCP dataset can be obtained from
487 <https://www.ncei.noaa.gov/products/climate-data-records/precipitation-gpcp-daily>.
488 Teleconnection indices can be found at <https://psl.noaa.gov/data/climateindices/list/>. The NCEP-
489 NCAR reanalysis is obtained from
490 <https://www.esrl.noaa.gov/psd/data/gridded/data.ncep.reanalysis2.html>.
491 The CALIPSO product is available at
492 [https://asdc.larc.nasa.gov/project/CALIPSO/CAL_LID_L3_Tropospheric_APro_AllSky-
493 Standard-V4-20_V4-20](https://asdc.larc.nasa.gov/project/CALIPSO/CAL_LID_L3_Tropospheric_APro_AllSky-Standard-V4-20_V4-20).

494
495 **Author contribution**

496 Y.L. and Y. Q. conceived of the presented idea. Y. Q., Y. W. and Y. L. developed the theory. Y.
497 L. performed the computations and verified the methods. Y. Q., Y. L. and K. Z wrote the first draft
498 of the manuscript. All authors contributed to the interpretation of the results and writing/revision
499 of the final manuscript.

500

501 **Competing interests**

502 Yun Qian and Hailong Wang are members of the editorial board of Atmospheric Chemistry and
503 Physics. The authors have no other competing interests to declare.

504

505 **Acknowledgments**

506 We benefited from discussing some aspects of this work with John M Wallace and Dae-Hyun Kim.
507 Yawen Liu is supported by the National Natural Science Foundation of China (No. 42325506).
508 ~~This study is also supported by the U.S. Department of Energy's Office of Science as part of the~~
509 ~~Regional and Global Modeling and Analysis program. This research is also supported by the US~~
510 ~~Department of Energy Office of Science Biological and Environmental Research as part of the~~
511 ~~Regional and Global Model Analysis and Multi-Sector Dynamics programme areas.~~ The Pacific
512 Northwest National Laboratory is operated for DOE by Battelle Memorial Institute under contract
513 DE-AC05-76RL01830. We are grateful to the High-Performance Computing (HPC) and the
514 Massive Data Center (MDC) at Nanjing University for the numerical calculations.

515

516

517

518

519 **References**

- 520 Abram, N. J., Henley, B. J., Sen Gupta, A., Lippmann, T. J. R., Clarke, H., Dowdy, A. J., Sharples, J. J., Nolan, R. H.,
521 Zhang, T. R., Wooster, M. J., Wurtzel, J. B., Meissner, K. J., Pitman, A. J., Ukkola, A. M., Murphy, B. P., Tapper, N.
522 J., and Boer, M. M.: Connections of climate change and variability to large and extreme forest fires in southeast
523 Australia, *Commun Earth Environ*, 2, ARTN 810.1038/s43247-020-00065-8, 2021.
- 524 Adler, R. F., Sapiano, M. R. P., Huffman, G. J., Wang, J. J., Gu, G. J., Bolvin, D., Chiu, L., Schneider, U., Becker,
525 A., Nelkin, E., Xie, P. P., Ferraro, R., and Shin, D. B.: The Global Precipitation Climatology Project (GPCP) Monthly
526 Analysis (New Version 2.3) and a Review of 2017 Global Precipitation, *Atmosphere*, 9, ARTN
527 13810.3390/atmos9040138, 2018.
- 528 Adler, R. W., Jian-Jian; Sapiano, Mathew; Huffman, George; Bolvin, David; Nelkin, Eric; and NOAA CDR Program:
529 Global Precipitation Climatology Project (GPCP) Climate Data Record (CDR), Version 1.3 (Daily), NOAA National
530 Centers for Environmental Information. doi:10.7289/V5RX998Z, 2017.
- 531 Aguilera, R., Corringham, T., Gershunov, A., and Benmarhnia, T.: Wildfire smoke impacts respiratory health more
532 than fine particles from other sources: observational evidence from Southern California, *Nature Communications*, 12,
533 ARTN 149310.1038/s41467-021-21708-0, 2021.
- 534 Amador, J. A., Alfaro, E. J., Lizano, O. G., and Magana, V. O.: Atmospheric forcing of the eastern tropical Pacific: A
535 review, *Prog Oceanogr*, 69, 101-142, 10.1016/j.pocean.2006.03.007, 2006.
- 536 Anthony Chen, A. and Taylor, M. A.: Investigating the link between early season Caribbean rainfall and the El Niño
537 + 1 year, *International Journal of Climatology*, 22, 87-106, 10.1002/joc.711, 2002.
- 538 Archibald, S.: Managing the human component of fire regimes: lessons from Africa, *Philosophical Transactions of
539 the Royal Society B: Biological Sciences*, 371, 20150346, 2016.
- 540 Athanasiadis, P. J., Wallace, J. M., and Wettstein, J. J.: Patterns of Wintertime Jet Stream Variability and Their
541 Relation to the Storm Tracks, *J Atmos Sci*, 67, 1361-1381, 10.1175/2009jas3270.1, 2010.
- 542 Bond, T. C., Doherty, S. J., Fahey, D., Forster, P., Berntsen, T., DeAngelo, B., Flanner, M., Ghan, S., Kärcher, B.,
543 and Koch, D.: Bounding the role of black carbon in the climate system: A scientific assessment, *Journal of Geophysical
544 Research: Atmospheres*, 118, 5380-5552, 2013.
- 545 Bowman, D. M., Balch, J. K., Artaxo, P., Bond, W. J., Carlson, J. M., Cochrane, M. A., D'Antonio, C. M., DeFries,
546 R. S., Doyle, J. C., and Harrison, S. P.: Fire in the Earth system, *science*, 324, 481-484, 2009.
- 547 Bowman, D. M. J. S., Williamson, G. J., Abatzoglou, J. T., Kolden, C. A., Cochrane, M. A., and Smith, A. M. S.:
548 Human exposure and sensitivity to globally extreme wildfire events, *Nat Ecol Evol*, 1, ARTN 005810.1038/s41559-
549 016-0058, 2017.
- 550 Cary, G. J., Keane, R. E., Gardner, R. H., Lavorel, S., Flannigan, M. D., Davies, I. D., Li, C., Lenihan, J. M., Rupp,
551 T. S., and Mouillot, F.: Comparison of the sensitivity of landscape-fire-succession models to variation in terrain, fuel
552 pattern, climate and weather, *Landscape ecology*, 21, 121-137, 2006.
- 553 **Chiodi, A. M., Potter, B. E., and Larkin, N. K.: Multi-Decadal Change in Western US Nighttime Vapor Pressure
554 Deficit, *Geophysical Research Letters*, 48, ARTN e2021GL092830.1029/2021GL092830, 2021.**
- 555 Crouse, J., DeCarlo, P., Blake, D. R., Emmons, L., Campos, T., Apel, E., Clarke, A., Weinheimer, A., McCabe, D.,
556 and Yokelson, R. J.: Biomass burning and urban air pollution over the Central Mexican Plateau, *Atmospheric
557 Chemistry and Physics*, 9, 4929-4944, 2009.
- 558 Crutzen, P. J. and Andreae, M. O.: Biomass Burning in the Tropics - Impact on Atmospheric Chemistry and
559 Biogeochemical Cycles, *Science*, 250, 1669-1678, DOI 10.1126/science.250.4988.1669, 1990.
- 560 Danabasoglu, G., Lamarque, J. F., Bacmeister, J., Bailey, D. A., DuVivier, A. K., Edwards, J., Emmons, L. K., Fasullo,
561 J., Garcia, R., Gettelman, A., Hannay, C., Holland, M. M., Large, W. G., Lauritzen, P. H., Lawrence, D. M., Lenaerts,
562 J. T. M., Lindsay, K., Lipscomb, W. H., Mills, M. J., Neale, R., Oleson, K. W., Otto-Bliessner, B., Phillips, A. S.,
563 Sacks, W., Tilmes, S., van Kampenhou, L., Versteinst, M., Bertini, A., Dennis, J., Deser, C., Fischer, C., Fox-
564 Kemper, B., Kay, J. E., Kinnison, D., Kushner, P. J., Larson, V. E., Long, M. C., Mickelson, S., Moore, J. K.,
565 Nienhouse, E., Polvani, L., Rasch, P. J., and Strand, W. G.: The Community Earth System Model Version 2 (CESM2),
566 *J Adv Model Earth Sy*, 12, ARTN e2019MS00191610.1029/2019MS001916, 2020.
- 567 Ding, K., Huang, X., Ding, A. J., Wang, M. H., Su, H., Kerminen, V. M., Petaja, T., Tan, Z. M., Wang, Z. L., Zhou,
568 D. R., Sun, J. N., Liao, H., Wang, H. J., Carslaw, K., Wood, R., Zuidema, P., Rosenfeld, D., Kulmala, M., Fu, C. B.,
569 Poschl, U., Cheng, Y. F., and Andreae, M. O.: Aerosol-boundary-layer-monsoon interactions amplify semi-direct

570 effect of biomass smoke on low cloud formation in Southeast Asia, *Nature Communications*, 12, ARTN
571 641610.1038/s41467-021-26728-4, 2021.

572 Duran-Quesada, A. M., Gimeno, L., and Amador, J.: Role of moisture transport for Central American precipitation,
573 *Earth Syst Dynam*, 8, 147-161, 10.5194/esd-8-147-2017, 2017.

574 Fang, K. Y., Yao, Q. C., Guo, Z. T., Zheng, B., Du, J. H., Qi, F. Z., Yan, P., Li, J., Ou, T. H., Liu, J., He, M. S., and
575 Trouet, V.: ENSO modulates wildfire activity in China, *Nature Communications*, 12, ARTN 176410.1038/s41467-
576 021-21988-6, 2021.

577 Fasullo, J. T., Rosenbloom, N., and Buchholz, R.: A multiyear tropical Pacific cooling response to recent Australian
578 wildfires in CESM2, *Science Advances*, 9, eadg1213, 2023.

579 Flannigan, M. D., Krawchuk, M. A., de Groot, W. J., Wotton, B. M., and Gowman, L. M.: Implications of changing
580 climate for global wildland fire, *International journal of wildland fire*, 18, 483-507, 2009.

581 Flannigan, M. D., Logan, K. A., Amiro, B. D., Skinner, W. R., and Stocks, B.: Future area burned in Canada, *Climatic
582 change*, 72, 1-16, 2005.

583 Gelaro, R., McCarty, W., Suarez, M. J., Todling, R., Molod, A., Takacs, L., Randles, C. A., Darmenov, A., Bosilovich,
584 M. G., Reichle, R., Wargan, K., Coy, L., Cullather, R., Draper, C., Akella, S., Buchard, V., Conaty, A., da Silva, A.
585 M., Gu, W., Kim, G. K., Koster, R., Lucchesi, R., Merkova, D., Nielsen, J. E., Partyka, G., Pawson, S., Putman, W.,
586 Rienecker, M., Schubert, S. D., Sienkiewicz, M., and Zhao, B.: The Modern-Era Retrospective Analysis for Research
587 and Applications, Version 2 (MERRA-2), *J Climate*, 30, 5419-5454, 10.1175/Jcli-D-16-0758.1, 2017.

588 Giglio, L., Randerson, J. T., and Werf, G. R.: Analysis of daily, monthly, and annual burned area using the fourth -
589 generation global fire emissions database (GFED4), *Journal of Geophysical Research: Biogeosciences*, 118, 317-328,
590 2013.

591 Gillett, N., Weaver, A., Zwiers, F., and Flannigan, M.: Detecting the effect of climate change on Canadian forest fires,
592 *Geophysical Research Letters*, 31, 2004.

593 Harris, I., Jones, P., Osborn, T., and Lister, D.: Updated high - resolution grids of monthly climatic observations -
594 the CRU TS3. 10 Dataset, *International Journal of Climatology*, 34, 623-642, 2014.

595 Hersbach, H., Bell, B., Berrisford, P., Hirahara, S., Horanyi, A., Muñoz-Sabater, J., Nicolas, J., Peubey, C., Radu, R.,
596 Schepers, D., Simmons, A., Soci, C., Abdalla, S., Abellan, X., Balsamo, G., Bechtold, P., Biavati, G., Bidlot, J.,
597 Bonavita, M., De Chiara, G., Dahlgren, P., Dee, D., Diamantakis, M., Dragani, R., Flemming, J., Forbes, R., Fuentes,
598 M., Geer, A., Haimberger, L., Healy, S., Hogan, R. J., Holm, E., Janiskova, M., Keeley, S., Laloyaux, P., Lopez, P.,
599 Lupu, C., Radnoti, G., de Rosnay, P., Rozum, I., Vamborg, F., Villaume, S., and Thepaut, J. N.: The ERA5 global
600 reanalysis, *Quarterly Journal of the Royal Meteorological Society*, 146, 1999-2049, 10.1002/qj.3803, 2020.

601 Huang, X., Ding, K., Liu, J. Y., Wang, Z. L., Tang, R., Xue, L., Wang, H. K., Zhang, Q., Tan, Z. M., Fu, C. B., Davis,
602 S. J., Andreae, M. O., and Ding, A. J.: Smoke-weather interaction affects extreme wildfires in diverse coastal regions,
603 *Science*, 379, 457-461, 10.1126/science.add9843, 2023.

604 Huffman, G. J., Bolvin, D. T., Nelkin, E. J., and Tan, J.: Integrated Multi-satellitE Retrievals for GPM (IMERG)
605 technical documentation, Nasa/Gsfc Code, 612, 2019, 2015.

606 Huffman, G. J., Bolvin, D. T., Braithwaite, D., Hsu, K.-L., Joyce, R. J., Kidd, C., Nelkin, E. J., Sorooshian, S., Stocker,
607 E. F., and Tan, J.: Integrated multi-satellite retrievals for the global precipitation measurement (GPM) mission
608 (IMERG), *Satellite Precipitation Measurement: Volume 1*, 343-353, 2020.

609 Ichoku, C., Ellison, L. T., Willmot, K. E., Matsui, T., Dezfuli, A. K., Gatebe, C. K., Wang, J., Wilcox, E. M., Lee, J.,
610 and Adegoke, J.: Biomass burning, land-cover change, and the hydrological cycle in Northern sub-Saharan Africa,
611 *Environmental Research Letters*, 11, 095005, 2016.

612 Jiang, Y. Q., Yang, X. Q., Liu, X. H., Qian, Y., Zhang, K., Wang, M. H., Li, F., Wang, Y., and Lu, Z.: Impacts of
613 Wildfire Aerosols on Global Energy Budget and Climate: The Role of Climate Feedbacks, *J Climate*, 33, 3351-3366,
614 10.1175/Jcli-D-19-0572.1, 2020.

615 Jolly, W. M., Cochrane, M. A., Freeborn, P. H., Holden, Z. A., Brown, T. J., Williamson, G. J., and Bowman, D. M.
616 J. S.: Climate-induced variations in global wildfire danger from 1979 to 2013, *Nature Communications*, 6, ARTN
617 753710.1038/ncomms8537, 2015.

618 Kanamitsu, M., Ebisuzaki, W., Woollen, J., Yang, S.-K., Hnilo, J., Fiorino, M., and Potter, G.: NCEP-DOE AMIP-II
619 Reanalysis (R-2), *B Am Meteorol Soc*, 83, 1631-1644, 2002.

620 Knorr, W., Dentener, F., Lamarque, J. F., Jiang, L. W., and Arneth, A.: Wildfire air pollution hazard during the 21st
621 century, *Atmos Chem Phys*, 17, 9223-9236, 10.5194/acp-17-9223-2017, 2017.

622 Koster, R. D., Darmenov, A. S., and da Silva, A. M.: The quick fire emissions dataset (QFED): Documentation of
623 versions 2.1, 2.2 and 2.4, 2015.

624 Kreidenweis, S. M., Remer, L. A., Brientjes, R., and Dubovik, O.: Smoke aerosol from biomass burning in Mexico:
625 Hygroscopic smoke optical model, *Journal of Geophysical Research: Atmospheres*, 106, 4831-4844, 2001.

626 Lee, Y. S., Collins, D. R., Li, R., Bowman, K. P., and Feingold, G.: Expected impact of an aged biomass burning
627 aerosol on cloud condensation nuclei and cloud droplet concentrations, *Journal of Geophysical Research:*
628 *Atmospheres*, 111, 2006.

629 Liu, Y. W., Zhang, K., Qian, Y., Wang, Y. H., Zou, Y. F., Song, Y. J., Wan, H., Liu, X. H., and Yang, X. Q.:
630 Investigation of short-term effective radiative forcing of fire aerosols over North America using nudged hindcast
631 ensembles, *Atmos Chem Phys*, 18, 31-47, 10.5194/acp-18-31-2018, 2018.

632 Lu, Z., Liu, X., Zhang, Z., Zhao, C., Meyer, K., Rajapakshe, C., Wu, C., Yang, Z., and Penner, J. E.: Biomass smoke
633 from southern Africa can significantly enhance the brightness of stratocumulus over the southeastern Atlantic Ocean,
634 *Proceedings of the National Academy of Science*, 201713703, 2018.

635 Magi, B., Rabin, S., Shevliakova, E., and Pacala, S.: Separating agricultural and non-agricultural fire seasonality at
636 regional scales, *Biogeosciences*, 9, 3003, 2012.

637 Marlon, J. R., Bartlein, P. J., Carcaillet, C., Gavin, D. G., Harrison, S. P., Higuera, P. E., Joos, F., Power, M., and
638 Prentice, I.: Climate and human influences on global biomass burning over the past two millennia, *Nature Geoscience*,
639 1, 697-702, 2008.

640 Mouillot, F. and Field, C. B.: Fire history and the global carbon budget: a 1×1 fire history reconstruction for the 20th
641 century, *Global Change Biology*, 11, 398-420, 2005.

642 Page, S. E., Siegert, F., Rieley, J. O., Boehm, H. D. V., Jaya, A., and Limin, S.: The amount of carbon released from
643 peat and forest fires in Indonesia during 1997, *Nature*, 420, 61-65, 10.1038/nature01131, 2002.

644 Pechony, O. and Shindell, D.: Fire parameterization on a global scale, *Journal of Geophysical Research: Atmospheres*,
645 114, 2009.

646 Perdigon-Morales, J., Romero-Centeno, R., Barrett, B. S., and Ordonez, P.: Intraseasonal Variability of Summer
647 Precipitation in Mexico: MJO Influence on the Midsummer Drought, *J Climate*, 32, 2313-2327, 10.1175/Jcli-D-18-
648 0425.1, 2019.

649 Power, M. J., Marlon, J., Ortiz, N., Bartlein, P. J., Harrison, S. P., Mayle, F. E., Ballouche, A., Bradshaw, R. H.,
650 Carcaillet, C., and Cordova, C.: Changes in fire regimes since the Last Glacial Maximum: an assessment based on a
651 global synthesis and analysis of charcoal data, *Climate dynamics*, 30, 887-907, 2008.

652 Prasad, V. K., Badarinath, K., and Eaturu, A.: Biophysical and anthropogenic controls of forest fires in the Deccan
653 Plateau, India, *Journal of Environmental Management*, 86, 1-13, 2008.

654 Randerson, J., Chen, Y., Werf, G., Rogers, B., and Morton, D.: Global burned area and biomass burning emissions
655 from small fires, *Journal of Geophysical Research: Biogeosciences*, 117, 2012.

656 Rogers, C. M. and Bowman, K. P.: Transport of smoke from the Central American fires of 1998, *Journal of*
657 *Geophysical Research: Atmospheres*, 106, 28357-28368, 2001.

658 Running, S., Q. Mu, M. Zhao. : MODIS/Terra Gross Primary Productivity 8-Day L4 Global 500m SIN Grid
659 V061, distributed by NASA EOSDIS Land Processes Distributed Active Archive Center,
660 <https://doi.org/10.5067/MODIS/MOD17A2H.061>. Accessed 2023-12, 2021.

661 **Su, W., Charlock, T. P., And, F. G. R., and Rutan, D.: Photosynthetically active radiation from Clouds and the Earth's**
662 **Radiant Energy System (CERES) products, *Journal of Geophysical Research: Biogeosciences*, 2007.**

663 Tosca, M., Randerson, J., Zender, C., Flanner, M., and Rasch, P. J.: Do biomass burning aerosols intensify drought in
664 equatorial Asia during El Nino?, *Atmospheric Chemistry and Physics*, 10, 3515-3528, 2010.

665 Tosca, M. G., Randerson, J. T., and Zender, C. S.: Global impact of smoke aerosols from landscape fires on climate
666 and the Hadley circulation, *Atmos Chem Phys*, 13, 5227-5241, 10.5194/acp-13-5227-2013, 2013.

667 van Marle, M. J. E., Kloster, S., Magi, B. I., Marlon, J. R., Daniau, A. L., Field, R. D., Arneth, A., Forrest, M., Hantson,
668 S., Kehrwald, N. M., Knorr, W., Lasslop, G., Li, F., Mangeon, S., Yue, C., Kaiser, J. W., and van der Werf, G. R.:
669 Historic global biomass burning emissions for CMIP6 (BB4CMIP) based on merging satellite observations with
670 proxies and fire models (1750-2015), *Geosci Model Dev*, 10, 3329-3357, 10.5194/gmd-10-3329-2017, 2017.

671 Veira, A., Lasslop, G., and Kloster, S.: Wildfires in a warmer climate: Emission fluxes, emission heights, and black
672 carbon concentrations in 2090–2099, *Journal of Geophysical Research: Atmospheres*, 121, 3195-3223, 2016.

673 Voulgarakis, A. and Field, R. D.: Fire influences on atmospheric composition, air quality and climate, *Current*
674 *Pollution Reports*, 1, 70-81, 2015.

675 Winker, D. M., Tackett, J. L., Getzewich, B. J., Liu, Z., Vaughan, M. A., and Rogers, R. R.: The global 3-D distribution
676 of tropospheric aerosols as characterized by CALIOP, *Atmos Chem Phys*, 13, 3345-3361, 10.5194/acp-13-3345-2013,
677 2013.

678 Yokelson, R., Urbanski, S., Atlas, E., Toohey, D., Alvarado, E., Crounse, J., Wennberg, P., Fisher, M., Wold, C., and
679 Campos, T.: Emissions from forest fires near Mexico City, *Atmos. Chem. Phys*, 7, 5569-5584, 2007.

680 Yokelson, R. J., Crounse, J., DeCarlo, P., Karl, T., Urbanski, S., Atlas, E., Campos, T., Shinozuka, Y., Kasputin, V.,
681 and Clarke, A.: Emissions from biomass burning in the Yucatan, *Atmospheric Chemistry and Physics*, 9, 5785, 2009.

682 Yue, S., Zhu, J., Chen, S., Xie, Q., Li, W., Li, L., Ren, H., Su, S., Li, P., and Ma, H.: Brown carbon from biomass
683 burning imposes strong circum-Arctic warming, *One Earth*, 5, 293-304, 2022.

684 Zhang, Y. W., Fan, J. W., Shrivastava, M., Homeyer, C. R., Wang, Y., and Seinfeld, J. H.: Notable impact of wildfires
685 in the western United States on weather hazards in the central United States, *P Natl Acad Sci USA*, 119, ARTN
686 e220732911910.1073/pnas.2207329119, 2022.

687 Zhong, Q. R., Schutgens, N., van der Werf, G., van Noije, T., Tsigaridis, K., Bauer, S. E., Mielonen, T., Kirkevåg, A.,
688 Seland, O., Kokkola, H., Checa-Garcia, R., Neubauer, D., Kipling, Z., Matsui, H., Ginoux, P., Takemura, T., Le Sager,
689 P., Remy, S., Bian, H. S., Chin, M., Zhang, K., Zhu, J. L., Tsyro, S. G., Curci, G., Protonotariou, A., Johnson, B.,
690 Penner, J. E., Bellouin, N., Skeie, R. B., and Myhre, G.: Satellite-based evaluation of AeroCom model bias in biomass
691 burning regions, *Atmos Chem Phys*, 22, 11009-11032, 10.5194/acp-22-11009-2022, 2022.

692